Chinese Chemical Letters 31 (2020) 2330–2332

Contents lists available at ScienceDirect

Chinese Chemical Letters

journal homepage: www.elsevier.com/locate/cclet

Communication

CeO_2 quantum dots doped Ni-Co hydroxide nanosheets for ultrahigh energy density asymmetric supercapacitors

Huiyu Duan[a,b], Tong Wang[a], Xinyi Wu[a], Ziyun Su[a], Jing Zhuang[a], Suli Liu[a,*], Rongmei Zhu[b,*], Changyun Chen[a,*], Huan Pang[b,*]

[a] Key Laboratory of Advanced Functional Materials of Nanjing, School of Environmental Science, Nanjing Xiaozhuang University, Nanjing 211171, China
[b] School of Chemistry and Chemical Engineering, Institute for Innovative Materials and Energy, Yangzhou University, Yangzhou 225009, China

ARTICLE INFO

Article history:
Received 18 December 2019
Received in revised form 23 May 2020
Accepted 1 June 2020
Available online 1 June 2020

Keywords:
Asymmetric supercapacitor
Electrochemical energy storage
Quantum dots
Transition metal hydroxides
Rare earth

ABSTRACT

By integrating the merits of lanthanide elements and quantum dots, we firstly design CeO_2 quantum dots doped Ni-Co hydroxide nanosheet *via* a controllable synthetic strategy, which exhibits a large specific capacitance (1370.7 F/g at 1.0 A/g) and a good cyclic stability (90.6% retention after 4000 cycles). Moreover, we assemble an aqueous asymmetric supercapacitor with the obtained material, which has an extremely high energy density (108.9 Wh/kg at 378 W/kg) and outstanding cycle stability (retaining 88.1% capacitance at 2.0 A/g after 4000 cycles).

It is widely known that transition metal hydroxides (TMHs) are attractive materials for the design of electrodes with application in electrocatalysis [1–6], electrochemical analysis [7–9] and electrochemical energy storage [10–18], arising from their metal hydroxyl host layers and anions that can balance the charges in their crystalline galleries. Both Ni and Co are important members of the transition elements, which means they are not expensive and suitable for applying as high-performance electrodes. Thus, Ni and Co based materials have become a popular cathode material for electrochemistry [19], particularly for electric energy storage [20–23]. That is probably because of Faradaic oxidation-reduction reactions with hydroxyl anions and large theoretical surface area. In a case, Wang's group synthesized 2-methylimidazole-derived Ni-Co LDH nanosheets and used for high-performance electrode material in hybrid supercapacitors [24]. Li and his group used CoS_x/Ni-Co LDH nanocages with rhombic dodecahedral structure for high-performance electrode of asymmetric supercapacitors [25]. Nonetheless, the poor intrinsic conductivity and low ion conductive rate of transition metal hydroxides restricted their actual application.

In recent years, quantum dots have attracted intensive researches in many fields, which are microscopic semiconductor particles of a few nanometers, having optical and electronic properties. They differ from normal particles owing to quantum mechanics [26], involving the interaction of electrons with a pseudopotential or random matrix [27]. Because of the unique electronic and physicochemical properties, such as their strong and tunable fluorescence emission properties, quantum dots have been widely applied in luminescence [28,29], bioimaging [30], solar cells [31] and photo-electrocatalysis [32]. Besides, due to their small size, quantum dots usually display very high-level exposure of active sites [33], which would bring accelerated electroactivity. Arising from the extraordinary characteristics of lanthanide elements, such as allowing faster electrons and protons transfer, when doped in poor conductors, their intrinsic conductivity usually can be enhanced [34]. That makes lanthanide elements been such widely applied in electrochemistry [35]. As an important member of lanthanide elements, Ce is widely applied in electrochemical energy storage [36] particularly because of the excellent oxidation-reduction abilities.

By integrating the merits of both lanthanide elements and quantum dots, herein CeO_2 quantum dots doped Ni-Co hydroxide nanosheet (denoted as CQNCH) was designed for the first time *via* a controllable synthetic strategy. CeO_2 particles in the form of quantum dots were homogeneously dispersed on ultrathin Ni-Co hydroxide nanosheets, which could remarkably boost the electrochemical performance. The CQNCH showed an outstanding specific capacitance (1370.7 F/g at 1 A/g) and a good cyclic stability. In addition, we assembled an aqueous asymmetric

* Corresponding authors.
E-mail addresses: niuniu_410@126.com (S. Liu), rmzhu@yzu.edu.cn (R. Zhu), cychen@njxzc.edu.cn (C. Chen), panghuan@yzu.edu.cn (H. Pang).

https://doi.org/10.1016/j.cclet.2020.06.001

supercapacitor (ASC) with CQNCH, presenting an extremely high energy density, which was up to 108.9 Wh/kg. Furthermore, this strategy can also be used to the controllable fabrication of other rare-earth elements oxides quantum dots doped transition metal hydroxides that could promote the development of electrochemical energy storage.

CQNCH was fabricated *via* a convenient method and schematically showed in Fig. 1 (more synthetic details in Supporting information). We found that the doping of CeO_2 particles in quantum dots size homogeneously dispersed on Ni-Co hydroxide nanosheets, which obviously changed the morphology and electrochemical properties.

X-ray diffraction (XRD) characterized the structure of CQNCH (Fig. S1a in Supporting information). The pattern confirmed the Ce-doped Ni-Co hydroxide nanosheets that consisted of $Ni(OH)_2$ (JCPDS No. 14-0117), $Co(OH)_2$ (JCPDS No. 51-1731) and CeO_2 (JCPDS No. 34-0394), which exhibited three main diffraction peaks corresponding to (001) plane of $Ni(OH)_2$, (001) and (002) planes of $Co(OH)_2$. Similar with our previous work, the strong characteristic peak in region of low angle contributed from the interlayer intervals, which suggested CQNCH a layered structure [37]. As shown in Fig. S1b, there were also two weak diffraction peaks, which corresponded to (111), (200) planes of CeO_2.

The oxidation state and chemical composition of CQNCH were analyzed by X-ray photoelectron spectroscopy (XPS). The survey spectrum was shown in Fig. 2a, indicating that Ni, Co, Ce, O, C and a small amount N (from ammonium and nitrate) were evident. Fig. S2a (Supporting information) showed the high-resolution of Ni 2p spectrum. It suggested two clear-cut peaks at 855 and 873 eV, which were assigned to the Ni $2p_{1/2}$ and Ni $2p_{3/2}$ signals of Ni(II) [38], as well as the two satellite peaks located at 861 and 879 eV. As shown in Fig. S2b (Supporting information), the high-resolution of Co 2p spectrum displayed two peaks at 781 eV and 796 eV, which could be assigned to Co $2p_{3/2}$ and Co $2p_{1/2}$ [39]. There were six peaks in Fig. 2b, referring to three pairs of spin-orbit doublets, which were denoted as v, v'', v''' that were contributed from Ce(IV) $3d_{5/2}$ and u, u'', u''' that were from Ce(IV) $3d_{5/2}$. Other signatures (denoted as v_0, v', u_0, and u') were ascribed to Ce(III) [27]. It is probably because the Ce(IV) was partly reduced to Ce(III) by dodecylamine.

The morphological features of CQNCH were revealed by scanning electron microscopy (SEM). Figs. 3a and b showed the SEM images of as-synthesized samples, which revealed the layered structure, in line with the result of XRD. Transmission electron microscopy (TEM) further disclosed the morphological features of CQNCH. The TEM images at different resolutions were shown in Figs. 3c and d, which further confirmed the paper-like layered structure. What is more, according to Fig. 3e, it clearly demonstrated that the CeO_2 was homogeneously dispersed on the surface of Ni-Co hydroxide nanosheets in the form of quantum dots. Comparing with Ni-Co hydroxide nanosheets (Fig. S3 in Supporting information), the doping of CeO_2 could make Ni-Co hydroxide nanosheets dispersed and prevent aggregation, which enabled CQNCH more exposure of active sites. The high-resolution TEM was shown in Fig. 3f, which unraveled one obvious lattice

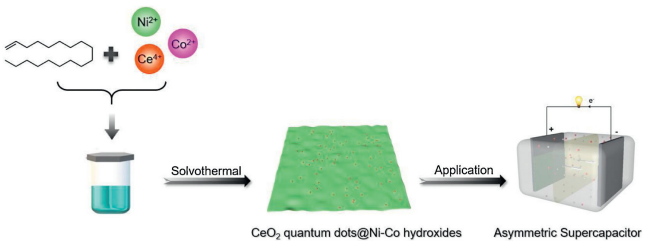

Fig. 1. Schematic illustration of the fabrication processes of CQNCH.

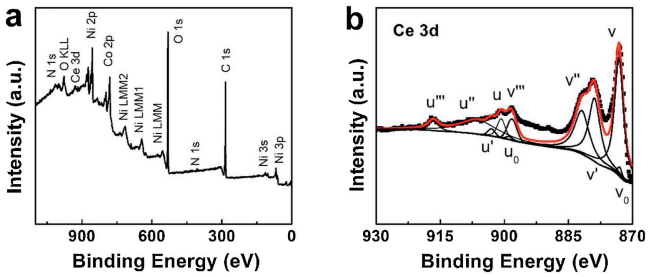

Fig. 2. (a) XPS spectrum of CQNCH. (b) High-resolution of Ce 3d XPS spectra.

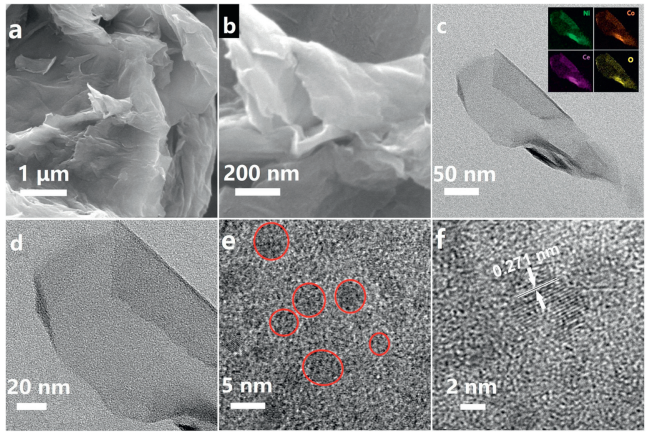

Fig. 3. (a, b) SEM image of the as-prepared CQNCH. (c) TEM image and elements mapping images of CQNCH. (d) TEM image of CQNCH. (e, f) HRTEM image of CQNCH.

fringe with an interplanar gap of 0.271 nm, completely corresponding to (200) plane of CeO_2. The corresponding elements mapping images were shown in Fig. 3c, which displayed Ni, Co and Ce were almost uniformly distributed in the CQNCH.

Different electrochemical analytic methods can be utilized to examine the electrochemical property of CQNCH. Cyclic voltammetry (CV) is a crucial technique to investigate the redox behavior of an electrode material, and the result was shown in Fig. S6a (Supporting information). The result of CV at scan rates ranging from 10 mV/s to 50 mV/s in a 3 mol/L KOH exhibited complex redox peaks, indicating the redox behavior consisted of $Co(OH)_2$ and $Ni(OH)_2$, with the existence of hydroxide ions. The clear redox peaks and large area of CV curves indicated the excellent faradic electrochemical reaction process, which led to a good pseudocapacitive performance.

The galvanostatic charge-discharge (GCD) curves of CQNCH within a voltage window of 0 to 0.4 V at 1.0–5.0 A/g were shown in Fig. S6b (Supporting information), in which the large current density peaks at all scan rates suggested the good pseudocapacitive behavior. The plateaus in the GCD curves indicated the presence of Faradaic processes, which were consistent with the CV scanning results. According to the GCD curves, the specific capacity of CQNCH was calculated to 1370.7, 1231.0, 1172.6, 1141.8 and 1120.5 F/g at current densities of 1.0, 2.0, 3.0, 4.0 and 5.0 A/g, respectively (Fig. S6c in Supporting information). For comparison, Fig. S5 showed the GCD curves of Ni-Co hydroxide nanosheets and the specific capacitance was also displayed in Fig. S6c, which demonstrated the doping of Ce obviously enhanced the supercapacitor performance of pristine Ni-Co hydroxide nanosheets.

It is significant for energy storage appliances to work with safety and stability in a long time, so the cycling stability test is very meaningful. As shown in Fig. S6d (Supporting information), we tested the cycling stability of CQNCH *via* constant cycling

(charge and discharge) at 2.0 A/g. In the first cycle, the capacitance of CQNCH was 1202.2 F/g. As the cycle number increased, the capacitance gradually enlarged and got the maximum of 1230.8 F/g at the 6th cycle. When cycled 1000 times, the capacitance declined to 1174.6 F/g. With the further increase of cycle number, the descending rate slowed down slightly. After 4000 cycles it finally faded to 1083.8 F/g, retaining more than 90.1% of its initial capacity at 2.0 A/g.

Additionally, we assembled the aqueous asymmetric supercapacitor device whose positive and negative electrodes were consisted of CQNCH and activated carbon, respectively (denoted as CQNCH//AC). The CV and GCD curves of CQNCH//AC at divergent scan rates were shown in Figs. 4a and b. The CQNCH//AC reached an ultrahigh energy density of 108.9 Wh/kg at 378 W/kg and remained 62.2 Wh/kg even at 4381 W/kg, which is significantly better than previously reported ASCs, such as CCO-NS//HCP-CNF (25.4 Wh/kg at 400 W/kg) [40], EC@$NiCo_2S_4$//EC (46.4 Wh/kg at 801 W/kg) [41], $CoNiSe_2$//AC (46.5 Wh/kg at 160.1 W/kg) [42], NCNs-0.1//AC (43.02 Wh/kg at 820.29 W/kg) [43], NA-LDH-OA-2//AC (40.26 Wh/kg at 943 W/kg) [8], PPC-800−2//PPC-800−2 (16.97 Wh/kg at 200 W/kg) [44]. Fig. 4c showed the corresponding comparison Ragone plots. What is more, the CQNCH//AC also exhibited satisfying cycling stability that retained more than 88.1% after 4000 cycles at 2 A/g (Fig. 4d). After stability test, the positive electrode materials were characterized by XRD again (Fig. S7 in Supporting information). According to Fig. S7, the peaks had no significant change, which suggested that the materials kept the initial structure after the stability test. The CV and GCD curves of AC were shown in Fig. S8 (Supporting information), which showed the capacity of 115.5 F/g at 1 A/g.

In conclusion, we fabricated a paper-like layered CeO_2 quantum dots doped Ni-Co hydroxide nanosheets *via* a simple one-step solvothermal method, which is low-cost, environment benign and convenient. The consequences exhibited that CQNCH presented an enhanced supercapacitor performance. CQNCH as an electrode material displayed an outstanding specific capacity of 1370.7 F/g at 1 A/g with more than 90.6% capacitance retention after 4000 cycles at 2 A/g. Moreover, the aqueous asymmetric supercapacitor (CQNCH//AC) device was assembled, which displayed an ultrahigh energy density of 108.9 Wh/kg at a power density of 378 W/kg and the capacitance retained 88.1% at 2 A/g after 4000 cycles. What is more, this strategy can be utilized to the controllable fabrication of other rare-earth elements oxides quantum dots doped transition metal hydroxides, which would accelerate the improvement of electrochemical energy storage device.

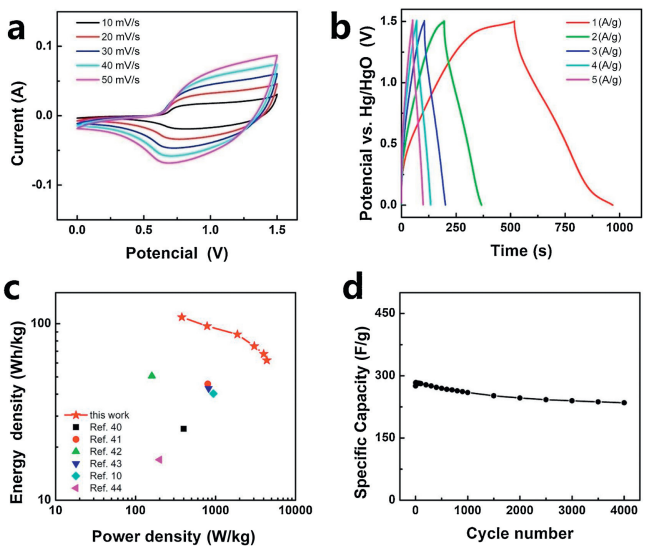

Fig. 4. (a) Cyclic voltammetry within a 0.15–0.55 V range at a scan rate 10–50 mV/s on the electrode in 3.0 mol/L KOH at room temperature. (b) Galvanostatic charge–discharge curves with current densities of 0.5–5.0 A/g. (c) Ragone plots of CQNCH//AC compared with those of the previous asymmetric supercapacitors; (d) Charge-discharge cycling test at 2.0 A/g.

Declaration of competing interest

The authors declare that they have no known competing financial interests or personal relationships that could have appeared to influence the work reported in this paper.

Acknowledgments

We acknowledge the financial supports of Natural Science Program of Nanjing Xiaozhuang University (No. 2018NXY22), 333 High-level Talents Cultivation Project of Jiangsu Province in 2018 (No. BRA2018101).

Appendix A. Supplementary data

Supplementary material related to this article can be found, in the online version, at doi:https://doi.org/10.1016/j.cclet.2020.06.001.

References

[1] J. Zhang, J. Liu, L. Xi, et al., J. Am. Chem. Soc. 140 (2018) 3876–3879.
[2] X.R. Li, J.L. Wei, Q. Li, et al., Adv. Funct. Mater. 28 (2018) 1800886.
[3] S.S. Zheng, B. Li, Y.J. Tang, et al., Nanoscale. 10 (2018) 13270–13276.
[4] S.S. Zheng, X.T. Guo, H.G. Xue, et al., Chem. Commun. 55 (2019) 10904–10907.
[5] H.Q. Liu, D.P. Zhao, Y. Liu, et al., Chem. Eng. J. 373 (2019) 485–492.
[6] B. Hu, J.Y. Yuan, J.Y. Tian, et al., J. Colloid Interf. Sci. 531 (2018) 148–159.
[7] W. Shi, J. Mao, X. Xu, et al., J. Mater. Chem. A. 7 (2019) 15654.
[8] X. Xu, W. Shi, W. Liu, et al., J. Mater. Chem. A. 6 (2018) 24086.
[9] Y. Luo, X. Guo, M. Yuan, et al., ACS Sustainable Chem. Eng. 7 (2019) 8972–8978.
[10] H. Zhang, M.U. Tahir, X.L. Yan, et al., Chem. Eng. J. 368 (2019) 905–913.
[11] B. He, Q.C. Zhang, P. Man, et al., Nano Energy 64 (2019) 103935.
[12] K.S. Huang, B. Li, M.M. Zhao, et al., Chin. Chem. Lett. 28 (2017) 2195–2206.
[13] W.H. Zuo, C.Y. Xie, P. Xu, Y.Y. Li, J.P. Liu, Adv. Mater. 29 (2017) 1703463.
[14] Z. Liang, R. Zhao, T. Qiu, R. Zou, Q. Xu, Energy Fuels 1 (2019) 100001.
[15] L. Jin, X.X. Li, C.S. Liu, H. Pang, Chin. Chem. Lett. (2019), doi:http://dx.doi.org/10.1016/j.cclet.2019.08.044.
[16] W.J. Ma, S.H. Chen, S.Y. Yang, et al., J. Power Sources 306 (2016) 481–488.
[17] S. Sun, T. Zhai, C.L. Liang, S.V. Savilov, H. Xia, Nano Energy 45 (2018) 390–397.
[18] Z.H. Wang, D.K. Denis, Z.W. Zhao, et al., J. Mater. Chem. A. 7 (2019) 18109–18117.
[19] H. Zhang, H.Y. Li, B. Akram, X. Wang, Nano Res. 12 (2019) 1327–1331.
[20] H. Pang, X.R. Li, Q.X. Zhao, et al., Nano Energy 35 (2017) 138–145.
[21] T. Nguyen, M. Boudard, M.J. Carmezim, M.F. Montemor, Sci. Rep. 7 (2017) 39980.
[22] S.Q. Wang, Z.Q. Zhu, P.W. Li, et al., J. Mater. Chem. A 6 (2018) 20015–20024.
[23] Z.L. Wang, Z.W. Zhao, Y.R. Zhang, et al., J. Alloys. Compd. 779 (2019) 81–90.
[24] T. Wang, S.L. Zhang, X.B. Yan, et al., ACS Appl. Mater. Interfaces 9 (2017) 15510–15524.
[25] X.H. Guan, M.H. Huang, L. Yang, G.S. Wang, X. Guan, Chem. Eng. J. 372 (2019) 151–162.
[26] Q. Wei, Y.H. Zhao, Q.M. Di, et al., J. Phys. Chem. C 121 (2017) 6152–6159.
[27] D.M. Zumbuhi, J.B. Miller, C.M. Marcus, et al., Phys. Rev. Lett. 89 (2002) 276803.
[28] F. Zhang, H.Z. Zhong, C. Chen, et al., ACS Nano 9 (2015) 4533–4542.
[29] X.X. Sheng, Y. Liu, Y. Wang, et al., Adv. Mater. 29 (2017) 1700150.
[30] M.A. Walling, J.A. Novak, J.R.E. Shepard, Int. J. Mol. Sci. 10 (2009) 441–491.
[31] A. Swarnkar, A.R. Marshall, E.M. Sanehira, et al., Science 354 (2016) 92–95.
[32] S.J. Xu, D. Li, P.Y. Wu, Adv. Funct. Mater. 25 (2015) 1127–1136.
[33] W. Huang, M. Xu, J. Liu, et al., Adv. Funct. Mater. 29 (2019) 1808762.
[34] S.L. Liew, Z. Zhang, T.W.G. Goh, et al., Int. J. Hydrogen Energy 39 (2014) 4291–4298.
[35] M.R. Wei, W. Che, H.Z. Li, et al., Appl. Surf. Sci. 484 (2019) 551–559.
[36] G. Manibalan, G. Murugadoss, R. Thangamuthu, et al., Appl. Surf. Sci. 456 (2018) 104–113.
[37] H.Y. Duan, S.S. Zheng, J. Zhuang, et al., ChemElectroChem 5 (2018) 3150–3154.
[38] M.C. Biesinger, B.P. Payne, L.W.M. Lau, A. Gerson, R.S.C. Smart, Surf. Interface Anal. 41 (2009) 324–332.
[39] U.M. Patil, S.C. Lee, J.S. Sohn, et al., Electrochim. Acta 129 (2014) 334–342.
[40] R. Suresh Babu, R. Vinodh, A.L.F. de Barros, et al., Chem. Eng. J. (2019) 390–403.
[41] Y.P. Liu, Z.L. Li, L. Yao, et al., Chem. Eng. J. (2019) 550–559.
[42] X. Shi, H. Wang, S. Ji, et al., Chem. Eng. J. (2019) 320–327.
[43] X.S. Feng, Y. Huang, C. Li, et al., Chem. Eng. J. (2019) 51–60.
[44] J. Guo, D.L. Wu, T. Wang, Y. Ma, Appl. Surf. Sci. 475 (2019) 56–66.